

ON THE MODELLING OF SWELL WAVE PENETRATION INTO TIDAL INLET SYSTEMS

Jacco Groeneweg¹, Joana van Nieuwkoop¹ and Yaron Toledo²

For the calculations of the Hydraulic Boundary Conditions in the framework of the Dutch Legal Flood Safety Assessment (WTI), wave statistics obtained at deeper water buoys need to be transformed to the toe of the dike using the wave action model SWAN. This transformation is particularly challenging in complex tidal inlet systems such as the Wadden Sea and the Western Scheldt in the Netherlands. Although various model improvements have been made in SWAN, particularly in the propagation and bottom friction dissipation, one of the unresolved issues is that the penetration of North Sea swell waves into the tidal inlets is still underestimated by SWAN. The goal of this study is to verify the hypothesis that nonlinear interactions, in particular the sub-harmonic triad interactions, play a major role in the transmission of energy from flats into the channel, and that this process can explain SWAN's under-prediction of wave energy penetration. Since SWAN or any other wave-action equation type models lacks the relevant physics to study this problem, the Boussinesq-type TRITON model is used as well to verify the hypothesis.

The conceptual idea, raised by Toledo (2013), is that sub-harmonic wave interactions between second harmonic and basic components generate a wave component of the same frequency as the primary component but at a wider angle of approach. As a consequence, the energy density spectra become directionally broader. From a series of idealized cases with monochromatic and bi-chromatic waves propagating up and down a slope we conclude that the TRITON model results confirm the conceptual idea of 2D nonlinear interactions. Both sub-harmonic wave interactions (to lower frequencies) and super-harmonic wave interactions (to higher frequencies) prove to be important. These insights can be applied to the situation with waves propagating on a tidal flat towards a channel. In case the basic components approach the channel under a sharp angle, such that they will not be able to enter the channel due to refraction, the sub-harmonic components could approach the channel under a less sharp angle and enter the channel. In our study a clear difference between the TRITON and SWAN energy density spectra in and across the channel is observed, as the 2D nonlinear interactions cannot be modeled with the co-linear 1D approach in SWAN.

The hypothesis that nonlinear interactions play a major role in the transmission of energy from flats into the channel is confirmed, at least for the cases considered in this study. Additional investigations are still required in order to quantify and generalize the effect of nonlinear interactions on this transmission of energy. In addition, it is recommended to extend the presently implemented three-wave interaction formulation in SWAN to account for directional super- and sub-harmonic interactions.

Keywords: wave modeling, nonlinear wave interactions, SWAN, Boussinesq-type wave model, TRITON

1. INTRODUCTION

In compliance with the Dutch Water Act the strength of the Dutch primary water defenses must be assessed periodically for the required level of protection, which, depending on the area, may vary from 100 to 30,000 year loads. These loads are determined on the basis of Hydraulic Boundary Conditions (HBC). These HBC are obtained by transforming wave statistics obtained at deeper water buoys to the toe of the water defense using the wave action model SWAN (Booij et al., 1999). This transformation is particularly challenging in complex tidal inlet systems such as the Wadden Sea and the Western Scheldt in the Netherlands. The upper panel of Figure 1 shows the geometry with tidal channels and flats in the eastern part of the Wadden Sea. Over the last couple of years significant improvements in the wave modeling with SWAN have been made (see e.g. Van der Westhuysen et al., 2012, Zijlema et al., 2012). One of the remaining issues is the underestimation by SWAN of the penetration of North Sea swell waves, in the range of 0.03 - 0.20 Hz, under storm conditions. This was observed in hindcasts of waves penetrating the Eastern Scheldt and the Dutch part of the Eastern Wadden Sea and illustrated for one instant during the storm of 9 November 2007 in Figure 2. The computed swell energy (in the range of 0.03 - 0.20 Hz) at measurement location UHW1, situated close to the primary sea defense, is significantly smaller than the measured swell energy at that location.

¹ Deltares, P.O. Box 177, 2600 MH Delft, The Netherlands,

² School of Mechanical Engineering, Center for Mediterranean Sea Studies, Tel-Aviv University, Israel.

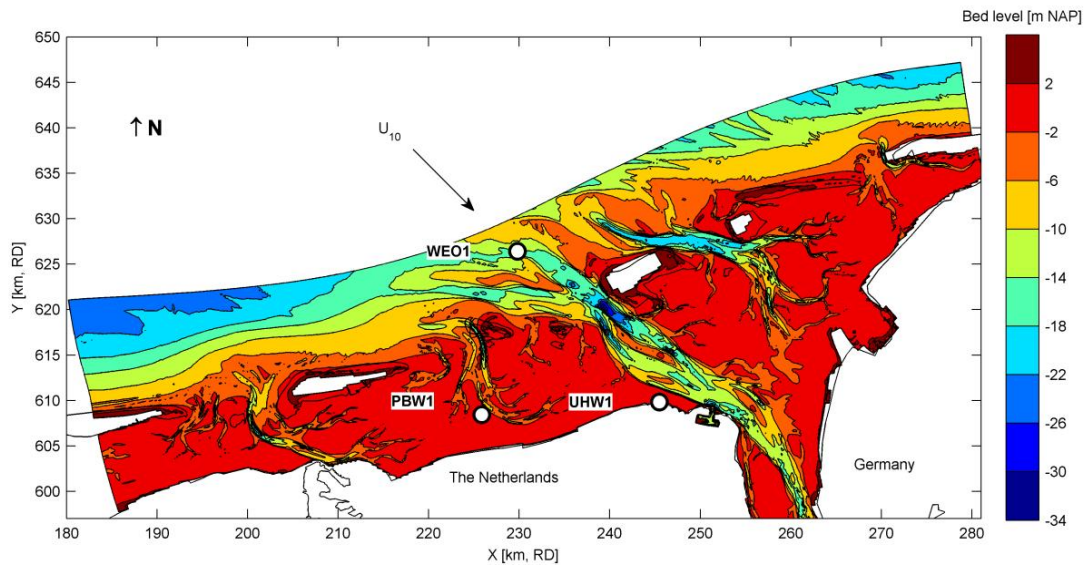


Figure 1: Depth profile of the Eastern Wadden Sea in the Netherlands (upper panel). WEO1, PBW1 and UHW1 indicate the locations of three wave rider buoys.

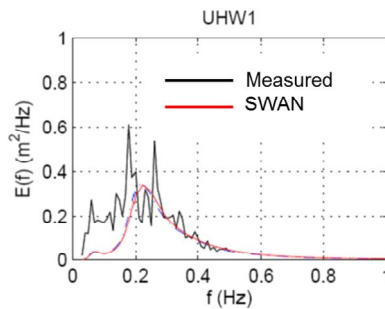


Figure 2: Measured and computed variance density at location UHW1 (see Figure 1) at 9 November 2007, 9:00h CET.

Previous analyses of the penetration of swell waves into the Dutch Eastern Wadden Sea have shown that the model-observation agreement improves if bottom friction is deactivated, the refraction on the low frequency waves is reduced, quadratic frequency-dependent wave breaking is applied and/or the water level is increased. Computations with both SWAN and PHAROS, the latter based on the mild-slope equations, showed that the effect of diffraction is local and has a negligible effect on the amount of energy that penetrates towards the mainland.

Laboratory experiments and successive computations with SWAN and the Boussinesq-type model TRITON (Borsboom et al., 2000) by Eslami et al. (2012) did not lead to the conclusion that SWAN overestimates refraction. Therefore, the hypothesis that the energy in SWAN will dissipate on the tidal flats before being able to reach the mainland was refuted. Hence, an explanation for the reported underestimation of the low frequency components could not be given.

In a comparison, using laboratory data obtained for a port entrance study, Groeneweg et al. (2014) found that the Boussinesq-type model TRITON (Borsboom et al., 2000) correctly predicted that the wave height hardly decreases, when waves propagate obliquely across a flat into a channel. However, SWAN predicts a sharp decrease of wave height across the flat-channel slope, due to refraction at the channel-flat interface. Toledo (2013) showed that two-dimensional nonlinear wave triad interactions have great importance in oblique wave incidence problems. In these problems, sub-harmonic two-dimensional triad interactions play a significant role as they are capable of transferring energy from higher frequencies to lower ones at larger attack angles than the original incident wave input. It appears that waves created by sub-harmonic waves have broader directionality comparing to the incident waves (see Herbers et al., 1995, for infra-gravity wave generation) and thus could provide a

mechanism by which energy is transferred over the flat-channel slope. This sub-harmonic energy transfer is not modeled in SWAN which only includes triad interaction transferring energy to higher harmonics in 1D.

The hypothesis is raised that two-dimensional nonlinear interactions (and especially the sub-harmonic interactions) play a major role in the transmission of energy from flats into navigation channels. Groeneweg et al. (2014) made plausible that this process can explain SWAN's under-prediction of wave energy penetration into a complex tidal inlet system. Since SWAN lacks the physics relevant for studying this problem, the TRITON model was used in order to verify the hypothesis. TRITON does include the two-dimensional nonlinear interactions, including the sub-harmonic interactions. The objective of the present paper is to give a theoretical explanation for SWAN's underestimation of swell penetration into channels and over complex geometries with tidal channels and flats in general.

After having given an initial explanation in the previous chapter, the problem at hand is further illustrated in Chapter 2 with the physical model and numerical model results of the laboratory experiments, also described in Groeneweg et al. (2014). In Chapter 3 a theoretical explanation for the observations in Chapter 3 is given by means of academic numerical experiments with TRITON. First of all the results of Toledo (2013) are reproduced by TRITON and results of further numerical experiments are presented to illustrate the role of non-linear interactions, in particular the directional broadening of the energy density spectrum in directional space. Further tests with monochromatic and bi-chromatic waves up-slope as well as down-slope, further illustrate the directional broadening. In Chapter 4 the effect of directional broadening of a full spectrum on the propagation of wave energy over tidal flats and into a tidal channels is presented, verifying the hypothesis that two-dimensional nonlinear interactions play a major role in the transmission of energy from flats into navigation channels. The paper ends with conclusions in Chapter 5.

2. LABORATORY EXPERIMENTS

In the Delta Basin of Deltares a 1:60 scale model was built, as sketched in Figure 3. A 0.38 m deep channel cuts through a 0.20 m deep horizontal plane. The side slopes of the channel are 1:5. At the western side of the model ($x = 0$ m) translatory wave paddles are able to generate regular and irregular waves, including directional spreading. The angle between the channel and the wave paddles is 65° . The northern and southern sides consist of vertical walls and at the eastern side a sloping beach damps out most of the wave energy. In front of the wave paddles the water depth is also 0.38 m. At a distance of 5 m from the wave paddles the water depth decreases over a 1:10 transitional slope to 0.20 m. Waves were measured at the eight locations shown in Figure 3, inside as well as on either side of the channel by using four standard resistance type wave gauges (denoted as WHM0x) and four directional wave gauges (denoted as WHM9x). As described in Groeneweg et al. (2014) six tests for various combinations of wave steepness (fixed significant wave height of 0.082 m and peak wave periods of 1.23 s, 1.45 s and 1.87 s) and directional spreading (0 and 20 degrees) were considered. The mean wave direction is 0 degrees (perpendicular to the wave paddles).

Both a SWAN and a TRITON model of the laboratory layout were set up for the same investigation. The computations presented here were performed using the SWAN model version 40.72ABCDE, in stationary third-generation mode. The physical settings are similar as those in Van der Westhuysen et al. (2012). The grid size is 0.10 m. For details about the model set-up, see Groeneweg et al. (2014). TRITON simulates, up to a certain accuracy (related to a specific depth range), the full nonlinear wave dynamics. To represent the primary waves and the higher order harmonics properly the TRITON simulations have been carried out on a fine grid with a resolution of 0.025 m in west-east direction, i.e. the mean wave direction, and 0.05 m in north-west direction. The time step is 0.025 s.

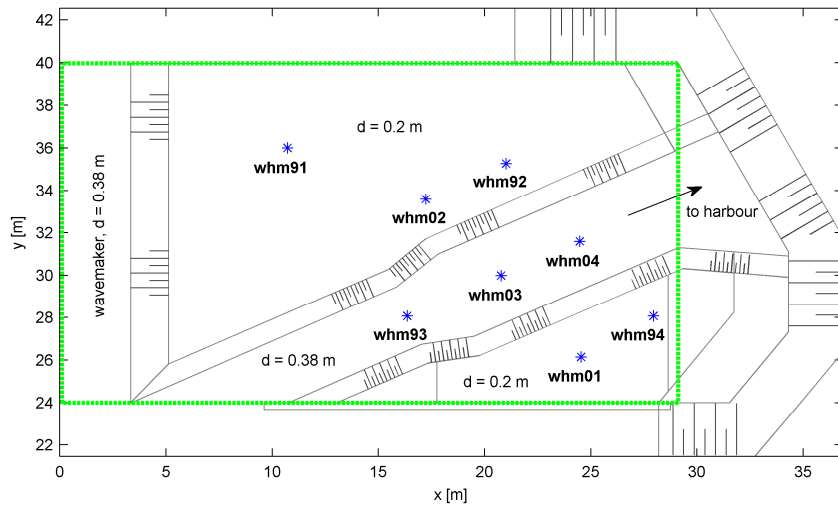


Figure 3: Layout of the physical model, including the locations of the resistance type wave gauges (whm0x) and directional wave gauges (whm9x). The green lines indicate the area of the computational domain.

SWAN and TRITON computations were done for all six tests. In Figure 4 the computed and measured energy density spectra for the test with directionally spread waves (dir. spr. = 20 degrees) with peak period $T_p = 1.87$ s are shown at two locations: Location whm91 at the shallow flat, upwave of the channel, and location whm93, inside the channel. Note that for all spectra the energy density above a certain threshold has been shown. In Figure 4 the threshold is $0.2 \cdot 10^{-5} \text{ m}^2/\text{Hz}/\text{deg}$. The computed spectra by TRITON and the measured spectra in the shallow region (whm91) are comparable. SWAN shows a slight overprediction of energy at the secondary peak. More interesting is the difference in results at location whm93. In the variance density spectra at the channel location whm93 the channel orientation is indicated by the solid line at 25 degrees. The measured and TRITON-computed variance density spectra at whm93 are comparable. SWAN on the other hand predicts no wave energy for wave components propagating under a sharp angle with the channel axis. Here refraction hampers the energy to penetrate into the channel. Apparently, an important physical mechanism is missing in SWAN, one that leads to an underprediction of wave energy inside the channel, and consequently also on the down-wave side of the channel. In Groeneweg et al. (2014) already the hypothesis was raised that 2D nonlinear interactions play an important role in the transmission of energy from the shallow region into a channel. In the next chapter a more theoretical explanation will be given, following the reasoning given in Toledo (2013).

3.THEORETICAL EXPLANATION

As already mentioned, Toledo (2013) addressed the importance of directional broadening of the wave energy spectrum. Toledo (2013) derived an oblique parabolic model, which is efficient but precludes wave reflections, and investigated the processes of linear and nonlinear shoaling of obliquely incident waves. In this chapter we first verify if the TRITON model can reproduce the parabolic model results of Toledo (2013). This assessment is a necessary verification of TRITON before we consider the cases we are interested in, being the downslope cases with regular (this chapter) and ultimately irregular waves over a more complex bathymetry with a channel (next chapter). Since the oblique parabolic model is not suited for the latter problem, the benchmark in this study is the TRITON model.

Reproduction of parabolic equation model results

Toledo (2013) considered two wave components with the same amplitude and wave period, but opposite wave directions with respect to the normal of the depth contours (i.e., in attack angles of $\pm\alpha$). The waves propagate from deep water to a shallow plateau over a constant bottom slope. He considered several angles of incidence (± 10 and ± 15 degrees), bottom slopes (1:5 and 1:10) and wave periods ($T = 2$ s and $T = 3$ s).

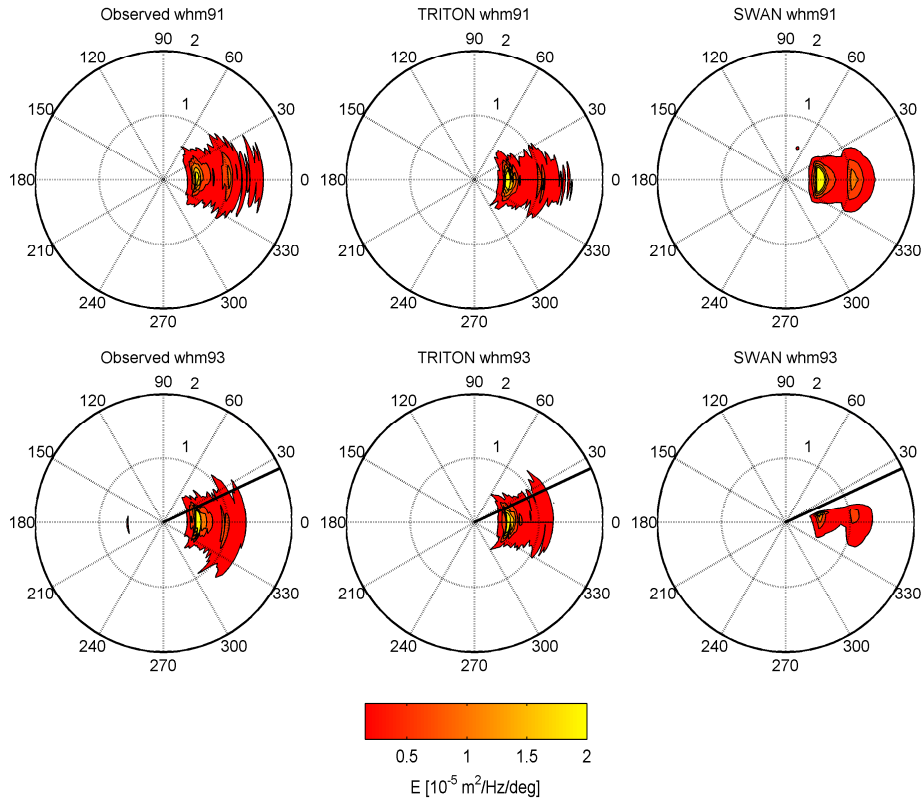


Figure 4: Observed and computed (TRITON and SWAN) 2D variance density spectra at the directional wave gauges whm91 (shallow flat) and whm93 (channel) for the initial condition $H_{m0} = 0.082$ m, $T_p = 1.87$ s, dir. spr. = 20 degrees. The solid black line in the whm93 spectra indicates the channel orientation.

TRITON and Toledo’s parabolic model use different simplifying assumptions, so their results will not be exactly the same. Since we are interested in reproducing the wave behavior, rather than the exact model results of Toledo (2013), we have limited ourselves to only one case. We considered the case of two monochromatic waves, both having the same amplitude $a = 0.01$ m and frequency ($f = 0.5$ Hz), but with different directions (15° and -15° with respect to the normal to depth contours).

The model set-up is similar to the set-up in Toledo (2013), in which at $x = 0$ the water depth is 10 m and a bottom slope starts, ending with a horizontal plateau at a water depth of 0.4 m. The computational domain of TRITON is decreased, by starting at 3 m depth instead of 10 m. This depth has been chosen because the relative depth kh ($k = 2\pi/L$ denotes the wave number, L is the wave length) for this depth is 3 and therefore the upper limit for the applicability range of TRITON (see Borsboom et al., 2000). Nevertheless, as $kh = 3$ still relates to deep water wave propagation this difference should not affect the results. In the presentation of the results the longitudinal direction (x) is taken relative to the deep-water wave length $L_0 = g/2\pi T^2$, with g the gravitational acceleration. For a wave period $T = 2$ s, $L_0 = 6.3$ m. With a slope of 1:5 the 3 m depth is reached at $x = 35$ m, or $x/L_0 = 5.6$. The computational domain ends at $x/L_0 = 14.4$. For $T = 2$ s the length of the domain is 55 m, see Figure 5.

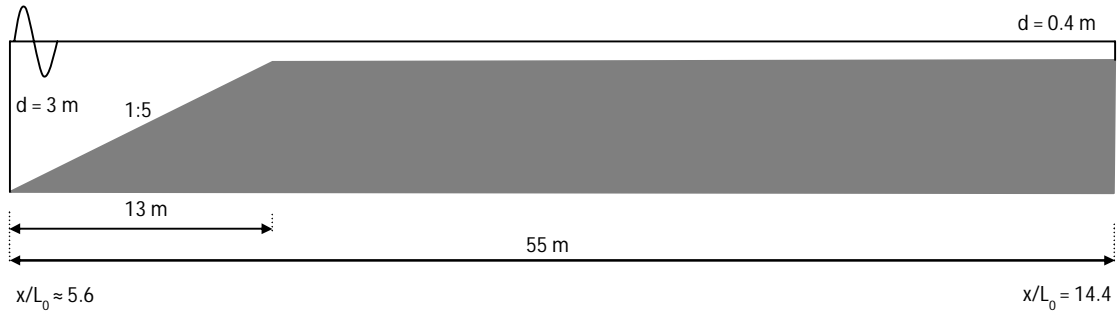


Figure 5: Set-up of the verification case, after Toledo (2013).

The domain needs to be wide enough such that reflections from the lateral boundaries, represented as vertical walls, do not influence the result. With the criterion that the area within 30 degrees from the boundary is influenced by boundary effects, the width needs to be at least 64 m. For post-processing, the domain needs to be wide enough to make a 2D f - k_y Fourier transform. Here k_y denotes the y -component of the wave number $k = (k_x, k_y)$. For the 2D-FFT a minimum of about 8 wave lengths is required. As the number of cells becomes very high with an increased width, the minimum of 8 wave lengths is chosen as domain width. For a 2 s wave propagating under 15 degrees with respect to the depth normal $k_y = 0.26$ rad/m at deep water. This leads to a required width of 200 meters.

The grid resolution has been chosen such that the third harmonic, which is the shortest of the three, is described by approximately 10 points. With $\Delta x = 0.1$ m and $\Delta y = 0.25$ m this criterion is almost satisfied. The third harmonic wave is described by only 7 grid points. Here this is considered to be just enough to correctly describe this wave component. To fulfill the CFL stability criterion a time step $\Delta t = 0.05$ s is required.

Along the incoming wave boundary at $x/L_0 = 5.6$ we have prescribed time series of surface elevations that are a summation of the single wave components. Besides generating waves, re-reflected waves are absorbed fully for components with the peak period and the undisturbed incoming wave direction. For other frequencies and directions the re-reflected components are reflected again to a small extent. At $x/L_0 = 14.4$ the boundary is defined as outflow boundary. Outflow boundaries in TRITON are optimized and fully transparent for waves with the peak period and the undisturbed incoming wave direction. For these wave conditions no wave energy is reflected back into the domain. Only a very limited amount of spurious wave energy will reflect off these boundaries when wave conditions at that boundary deviate from the prescribed values. This means that a small part of the outgoing waves may be reflected back into the domain from the outflow boundary. For practical applications this amount is very small and does not influence overall results. The two lateral boundaries at $y = 0$ m and $y = 200$ m are closed walls. The closed boundaries reflect 100% of the wave energy back into the domain. Note that Toledo (2013) did not have to impose side walls but could solve the infinite case as he used a quasi-two-dimensional model formulation for the numerical calculations.

To process the TRITON time series a Fast Fourier Transform (FFT) has been applied. For the numerical experiment considered the wave components mentioned in Table 1 are of interest. We use the same notation as in Toledo (2013) with φ the velocity potential and the first and second subscripts denoting the harmonic in frequency space and k_y – space respectively. Different wave components exist having the same frequency.

Table 1. Interactions between two wave components transferring energy to a third.		
Generated component	From harmonic interaction between components	For case $T = 2$ s
$\varphi_{1,\pm 1}$	Primary components	energy at $f = 0.5$ Hz
$\varphi_{1,\pm 3}$	sub harmonic: $\varphi_{2,2}$ and $\varphi_{1,-1}$ or $\varphi_{2,-2}$ and $\varphi_{1,1}$	energy at $f = 0.5$ Hz
$\varphi_{2,0}$	super harmonic: $\varphi_{1,1}$ and $\varphi_{1,-1}$	energy at $f = 1.0$ Hz
$\varphi_{2,\pm 2}$	super harmonic: $\varphi_{1,1}$ and $\varphi_{1,1}$ or $\varphi_{1,-1}$ and $\varphi_{1,-1}$	energy at $f = 1.0$ Hz
$\varphi_{3,\pm 1}$	super harmonic: $\varphi_{2,2}$ and $\varphi_{1,-1}$ or $\varphi_{2,-2}$ and $\varphi_{1,1}$	energy at $f = 1.5$ Hz
$\varphi_{3,\pm 3}$	super harmonic: $\varphi_{2,2}$ and $\varphi_{1,1}$ or $\varphi_{2,-2}$ and $\varphi_{1,-1}$	energy at $f = 1.5$ Hz

We have applied a 2D-FFT on time series in the y -direction to create a f - k_y spectrum for different values of x . From the 2D-FFT signal the variance density E was calculated as follows:

$$E(f, k) = \frac{1}{\Delta f \Delta k_y n_t^2 n_y^2} G_{\frac{N_t}{2}, \frac{N_y}{2}} G_{\frac{N_t}{2}, \frac{N_y}{2}}^*$$

with $n_t = N_t \Delta t$ the length of the time record, N_t the number of data points in the time record and Δt the sampling rate. Likewise $n_y = N_y \Delta y$ denotes the length of the y -transect, N_y the number of data points in the y -transect and Δy the distance between the data points.

The integration over f and k_y was done every meter in x -direction, in the center of the computational domain, to create a cross-shore evolution of the amplitude. Subsequently, the amplitude was normalized by the amplitude $A_{\phi_{1,1,0}}$ of the primary component $\phi_{1,1}$ at the offshore wave boundary, in our case at $x/L_0 = 5.6$. The variation along the centerline of the domain ($y = 100$ m) of the normalized amplitudes of the components mentioned in Table 1 are given in Figure 6. The qualitative agreement with the results of Toledo (2013, Fig. 7) is good for all wave components. The variation in the amplitude of the primary wave component is less than 5%. Nevertheless, after $x/L_0 = 7$, when reaching shallow water, the amplitudes of the higher harmonic components clearly increase, due to nonlinear interactions. The increase of the $\phi_{1,3}$ wave component is significant. The fluctuations in amplitudes are due to the fact that there is no full resonance. Because of the flat bed energy is transferred back and forth.

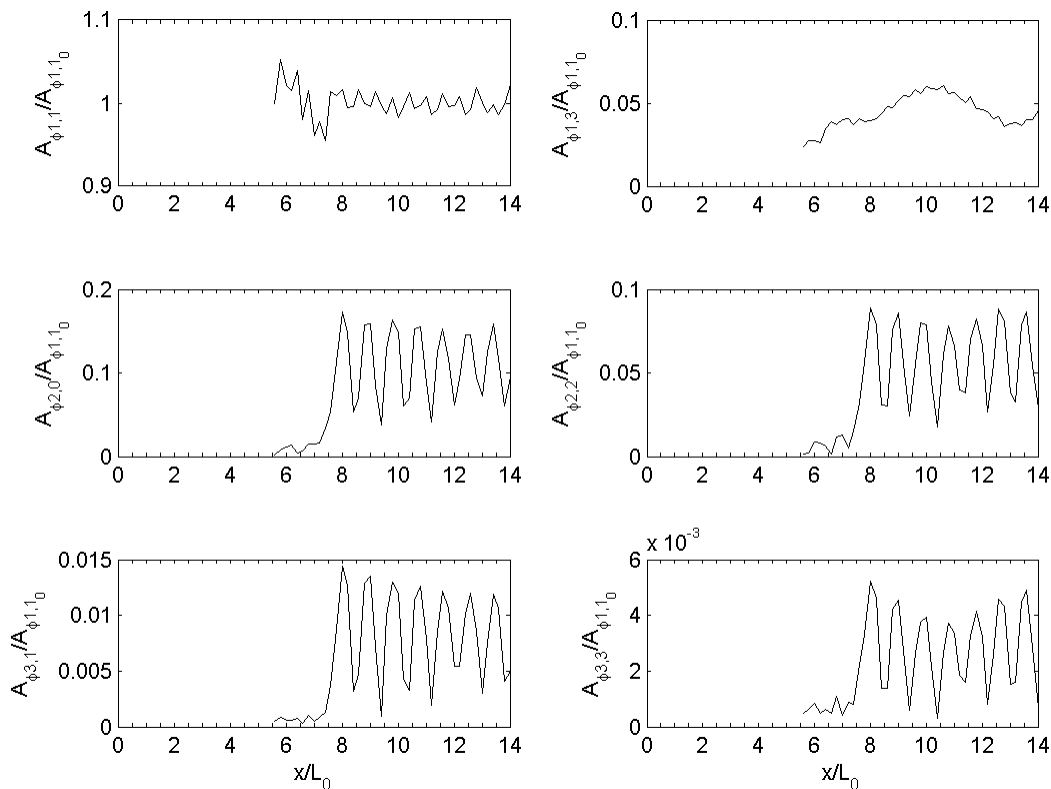


Figure 6: The variation in x -direction of the normalized amplitudes for the case of two single frequency wave components ($T = 2$ s) under opposite wave directions (± 15 degrees w.r.t. depth normal).

Figure 7 shows the f - k_y spectrum at $x/L_0 = 11.6$, on the plateau. The white arrows indicate the possible super-harmonic interactions, the red and purple arrows possible sub-harmonic interactions, as indicated in Table 1. The shoaling process of the primary components $\phi_{1,\pm 1}$ transfers energy via a nonlinear super-harmonic self-interaction to its double-harmonic components $\phi_{2,\pm 2}$. These components can be bound to the primary component and propagate at the same speed. Nevertheless, during the shoaling process due to changes in the bottom profile they can both grow and become freely propagating waves. The higher order components propagate in smaller attack angles comparing to the

primary component, as was already illustrated by Toledo (2013, Figures 4d, 5d, 6d and 10). This higher harmonic wave component ($\phi_{2,\pm 2}$) interacts with the oppositely angled primary wave component ($\phi_{1,\mp 1}$) via a nonlinear sub-harmonic resonance closure, indicated with the red arrows in Figure 7. This sub-harmonic interaction creates a first-harmonic wave component ($\phi_{1,\pm 3}$). Furthermore, the propagation angle of this first-harmonic wave component is much larger than the angle of the original primary incident waves (i.e., it has larger absolute k_y value). Figure 7 shows that the attack angle more than doubles, from 8° to 25° at location $x/L_0 = 11.6$, i.e. after shoaling/refraction. From this simplified problem, it was concluded that the directional range was broadened due to nonlinear shoaling, consistent with the infra-gravity results of Herbers et al. (1995).

Note that another combination of two-dimensional super- and sub-harmonic nonlinear triad interaction mechanism transfers energy to the $\phi_{1,\pm 3}$ wave components. This is a weaker mechanism in the presented case as it requires several super-harmonic interactions. It includes the super-harmonic interaction between the two primary incident waves ($\phi_{1,\pm 1}$) to create a second-harmonic directly incident wave ($\phi_{2,0}$). This second harmonic component has a sub-harmonic interaction with the third harmonic components $\phi_{3,\pm 3}$, (which were created in super-harmonic triad interactions between $\phi_{1,\pm 1}$ and $\phi_{2,\pm 2}$) to transfer energy to the $\phi_{1,\pm 3}$ wave components. These sub-harmonic interactions are marked in Figure 7 with purple arrows.

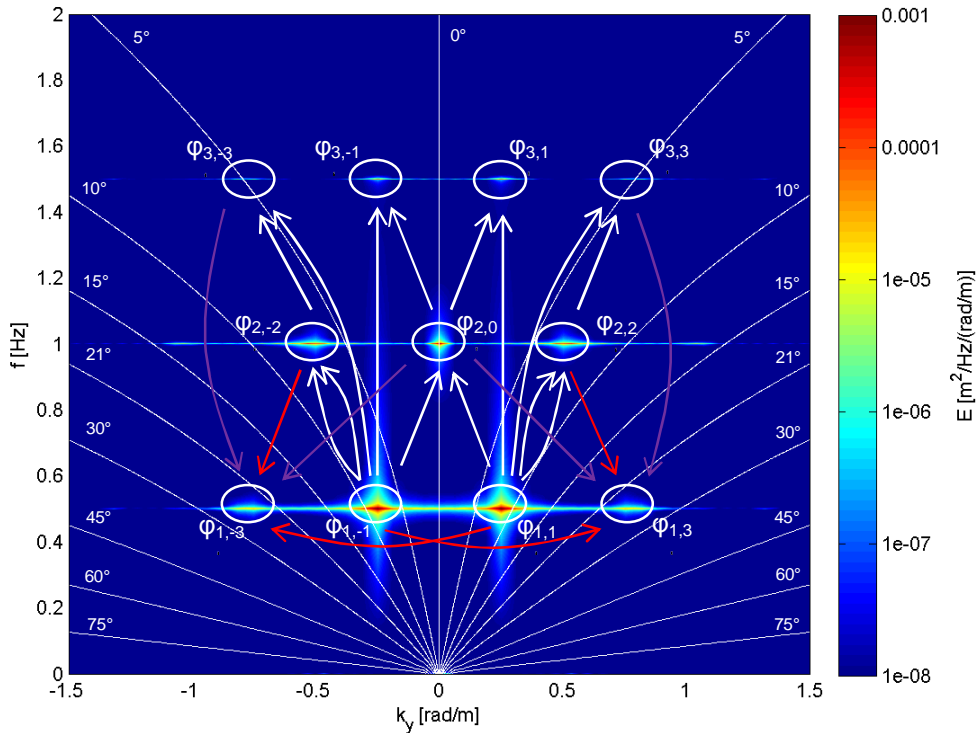


Figure 7: f - k_y variance density spectrum at $x/L_0 = 11.6$ for the case of two single frequency wave components ($T = 2$ s) under opposite wave directions (± 15 degrees w.r.t. depth normal). The white isolines indicate the combinations of equal propagation angle w.r.t. normal of the depth contours. The arrows indicate the interacting components.

More upslope verification cases

Apart from the “single frequency, two directions” simulation mentioned in the previous section, additional verifications with TRITON have been carried out, where waves propagate up a constant bottom slope and further onto a horizontal plateau. These computations concern “double frequency, two directions” (imposing the second harmonic at the boundary), “single frequency, one direction” and “double frequency, one direction”. In the latter case the two frequencies differ slightly, resulting in a low-frequency sub-harmonic component. Additionally, tests with a 100 times smaller amplitude were done. The results will not be presented and discussed here in detail. We draw the following conclusions from these computations:

- The conceptual idea of nonlinear interactions raised by Toledo (2013) has been confirmed for the more general cases mentioned above: Both sub-harmonic wave interactions and super-harmonic wave interactions prove to be important.
- By reducing the amplitude by a factor 100 the effect of nonlinear interactions decreases significantly. This aids in identifying the role of nonlinear interactions in the shoaling process.
- Imposing at the inflow boundary wave energy at the double frequency increases the nonlinear interactions between the various wave components, and the energy at the resulting sub- and super-harmonics.
- Sub-harmonic wave interactions between second harmonic and basic components clearly show only in the bi-directional cases the generation of a wave component of the same frequency as the primary component ($\phi_{1,\pm 3}$). Hence, an initial angular spreading of the wave field is necessary to get sub-harmonic wave interactions.

Oblique wave propagation across a flat-channel transition

In the previous section, we verified that the TRITON model captures the essential super- and sub-harmonic interaction processes when obliquely-incident waves propagate on a slope. This includes the $\phi_{1,\pm 3}$ components, which may be the agents that transmit energy across a flat-channel transition, i.e. down a slope. This configuration is investigated in this section. It is the next step towards more complex geometries with tidal flats and channels. The same input conditions are considered in this section as in the previous one: monochromatic and bi-chromatic waves approaching from two directions.

The setup is similar to the previous chapter with waves propagating first over a shallow horizontal bed and then down a 1:5 slope to a deeper horizontal bed resembling a channel. The model's geometry is presented in Figure 8. The depth is uniform in y-direction. At the inflow boundary the water is shallow with a depth of 0.2 m. After 9.1 m the depth increases via a 1:5 slope to 0.38 m. The depth values coincide with the values applied in the laboratory measurements presented, see Figure 3. The total length of the domain is 30 m, where in the last 20 m the bed is horizontal.



Figure 8: Geometry of down-slope verification cases.

The waves are reflected from the closed side walls. Given the 15 degrees incoming wave direction, the reflected waves affect an area of 15 m from the side wall at the end of the domain. For all tests the width of the basin is taken as 60 m. The wave period of the primary components is 2 s. The grid resolution has been chosen such that the third harmonic, which has the shortest wavelength of the three, is resolved by approximately 10 points per wavelength. With $\Delta x = 0.1$ m this criterion is almost satisfied, since the third harmonic wave has only 7 points per wave length. Here this is considered to be just enough to correctly describe this wave component. A time step $\Delta t = 0.1$ s is sufficient to fulfill the Courant criterion.

The same input conditions are considered in this section as in the previous one: monochromatic and bi-chromatic waves approaching from two directions, defining the following two cases:

- Case 1 (single frequency, two directions): $f_1 = 0.5$ Hz, $\theta_{1,\pm 1} = \pm 15^\circ$
- Case 2 (double frequency, two directions): $f_1 = 0.5$ Hz, $\theta_{1,\pm 1} = \pm 15^\circ$; $f_2 = 1.0$ Hz, $\theta_{2,\pm 2} = \pm 13.4^\circ$

Compared to the up-slope cases in the previous section the depth at the inflow boundary is much smaller for the cases in this section, 3 m versus 0.2 m. As a result the nonlinear interactions are much stronger right from the boundary on. This can be seen also by inspecting the Ursell number, which is a measure for nonlinearity and calculated here as $U_r = HL^2 / h^3$, with H the wave height, L wave length and h water depth: in the shallow part the Ursell number equals 18 and in the deeper part 4.8.

The variation in x -direction of the normalized amplitudes is given in Figure 9 for both Case 1 and Case 2. In Case 1 the basic components generate the second harmonics, which have zero energy at the boundary but increase in energy quickly. Super-harmonic interactions between the basic components and the second harmonics create the third harmonics. At the same time sub-harmonic interactions generate the $\phi_{1,\pm 3}$ components. There is no energy input in these components. Still, nonzero values appear at $x = 0$ m as the imposed input conditions do not satisfy the wave flow conditions in shallow water. Therefore, the system adjusts itself to satisfy the flow conditions by injecting energy to these components.

In Case 2 energy at the second harmonic is imposed at the boundary. Due to interaction with the basic component, the second harmonic loses energy when waves propagate further into the domain. The $\phi_{1,\pm 3}$ components vary slowly along the basin, except in the area of the slope. The bathymetry variations have a strong impact on both sub- and super-harmonic interactions between the basic components and second harmonics. In the deeper part, down-wave of the slope, the variation in the normalized amplitudes is small.

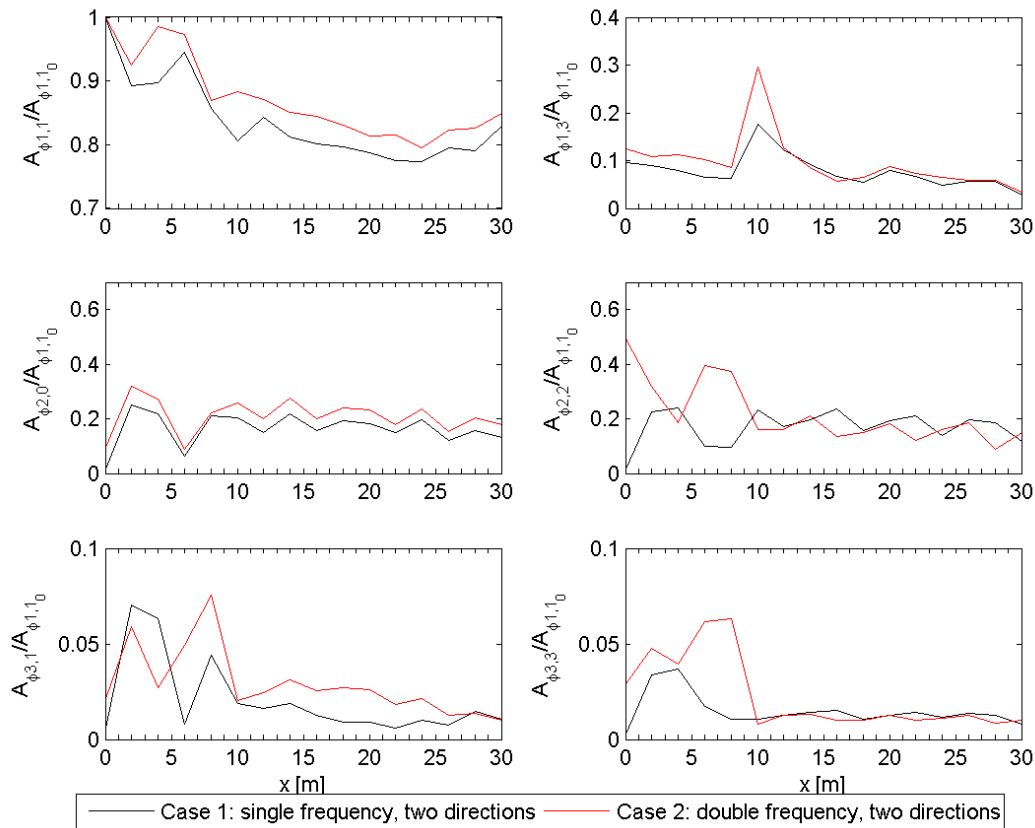


Figure 9: The variation in x -direction of the normalized amplitudes for Case 1 (black, single frequency, two directions) and Case 2 (red, double frequency, two directions) for the down-slope situation.

We may conclude that in the shallow area the nonlinear interactions are very strong. The super- and sub-harmonic interactions cause a significant shift of energy to both higher harmonics and to the sub-harmonic-generated $\phi_{1,\pm 3}$ components. Clearly, the spectra broaden significantly in frequency and directional space. This, as hypothesized, would allow for a transmittance of energy over a flat-channel interface.

4. VERIFICATION FOR A FULL SPECTRUM ACROSS A CHANNEL

In the previous chapter the focus was on the nonlinear interaction mechanism and generation of super- and sub-harmonics. In order to quantify the effect of this mechanism for the propagation of waves into the Wadden Sea, Groeneweg et al. (2014) considered various angles of incidence, with respect to the channel orientation. The reason for this is that in some cases swell wave components might refract on the channel slope and will not cross into the channel, whereas in other cases sub-

harmonic waves approaching the channel, even under a small attack angle, might transmit wave energy that enters and even crosses the channel via nonlinear super- and sub-harmonic interactions.

For a number of conditions both TRITON and SWAN computations were performed by Groeneweg et al. (2014). The conditions are based on the laboratory measurements, described in Groeneweg et al. (2014), see also Chapter 2. Here we consider only one condition, in order to illustrate the importance of nonlinear wave interactions in irregular sea states. At the offshore boundary a Jonswap spectrum is imposed, having a significant wave height $H_{m0} = 0.082$ m, peak period $T_p = 1.45$ s, directional spreading of 20 degrees and peak enhancement factor $\gamma = 3.3$. The mean wave direction is 0 degrees, i.e. perpendicular to the wave paddles.

The bathymetry for the computations is a simplified version of the laboratory tests reported in Groeneweg et al. (2014). In the lab tests the channel reflected an existing harbour approach channel and was widened towards the end. For analysis purposes this widening was removed so that the channel is straight. The geometry is presented in Figure 10. The waves are propagating from the offshore boundary at $x = 0$ m at a depth of 0.38 m to a transitional 1:10 ramp. The shallow region is 0.20 m. The oblique channel slope of 1:5 leads again to a water depth of 0.38 m. The computational domain in x -direction is 20 m and in y -direction 10 m. The y -coordinates show an offset of 26 m, which is the same as in the original laboratory tests.

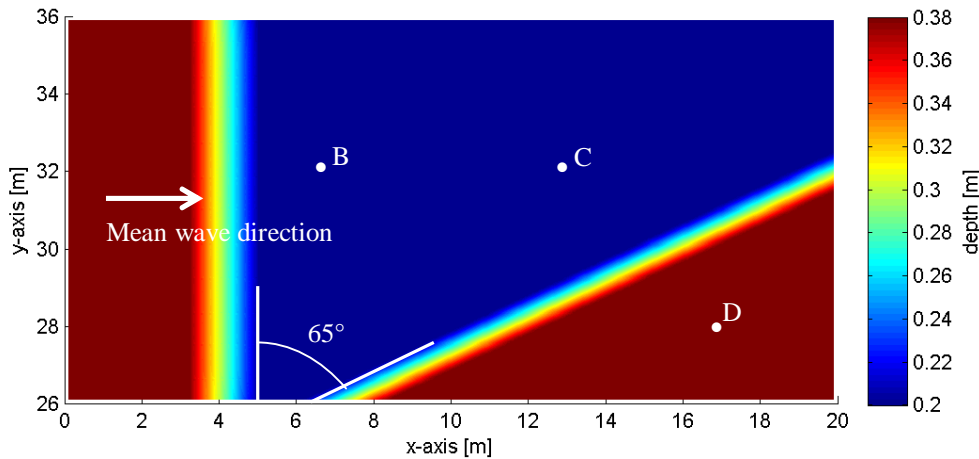


Figure 10: Bathymetry for the simplified channel case.

The TRITON grid resolution was chosen such that the third harmonic components are described by at least 10 grid points, resulting in $\Delta x = 0.025$ m and $\Delta y = 0.05$ m. The time step is $\Delta t = 0.025$ s, satisfying the Courant criterion. The Ursell numbers are significantly larger than 1, which implies a nonlinear regime both in the deep and shallow parts. Furthermore, for the third harmonic $kh = 6$ in the deep parts, which is beyond the limit of $kh = 3$ for which TRITON accurately determines the dispersion of the waves. However, for the qualitative purpose of this chapter this is acceptable. This is also supported by the fact that in deep water the Jonswap spectrum consists of limited energy in the higher frequencies. Energy is transferred to these frequencies through nonlinear triad interactions that take place at shallower depths ($kh < 3$), which agrees with TRITON's assumptions. The duration of the numerical experiment is set at 1500 s including a start-up period, which means that 1000 waves are considered. This duration is sufficient for a proper spectral analysis.

At the offshore boundary $x = 0$ m a Jonswap spectrum has been imposed. Internally TRITON transforms this spectrum into a time series along the entire offshore boundary. As mentioned in previous sections the boundary condition formulated in TRITON includes absorption of re-reflected waves. The two side boundaries at $y = 26$ m and $y = 36$ m are closed. The boundary at $x = 20$ m is an outflow boundary. The energy at the peak frequency of 1.5 s is absorbed. Energy at other frequencies is partly reflected.

The computations presented here were performed using the SWAN model version 40.72ABCDE, in stationary third-generation mode. The geographical resolution in both directions is 10 cm. The full directional circle is resolved with 1.5° directional bins. A frequency range of 0.4 – 2.5 Hz is

considered with a logarithmic distribution of the frequencies. The physical settings are similar to the settings in Section 2.

In Figure 11 the 2D variance density spectra computed by TRITON and SWAN have been presented at three locations: at locations B and C in the shallow region and at location D in the deep part, down-wave of the slope. Comparing the variance density spectra computed by TRITON at the shallow locations B and C, the variance density spectrum at location C shows more directional variation, due to wave reflection against the channel slope. Compared to TRITON the transfer to the second harmonic in SWAN is overpredicted across the transitional slope, which can be observed from the spectra near $f = 1.3$ Hz at locations B and C, and becomes even clearer when inspecting the 1D variance density spectra (not shown here). The LTA formulation (Eldeberky, 1996) in SWAN is a nonlinear self-interaction triad formulation, which means that a wave component only interacts with itself. Energy from the wave component under consideration is transferred to its corresponding second harmonic via super-harmonic interaction. TRITON however allows interactions between all wave components from all directions. The 2D super- and sub-harmonic interactions are spreading the energy over a range of frequencies and directions. The 1D approach in SWAN shows no spreading in directional space and only an increase of the energy of the second harmonic. The effect of the LTA is further illustrated in Groeneweg et al. (2014) by de-activating the LTA. By deactivating the LTA, the spectral shape hardly changes over the transitional slope and no energy is transferred to the second harmonic.

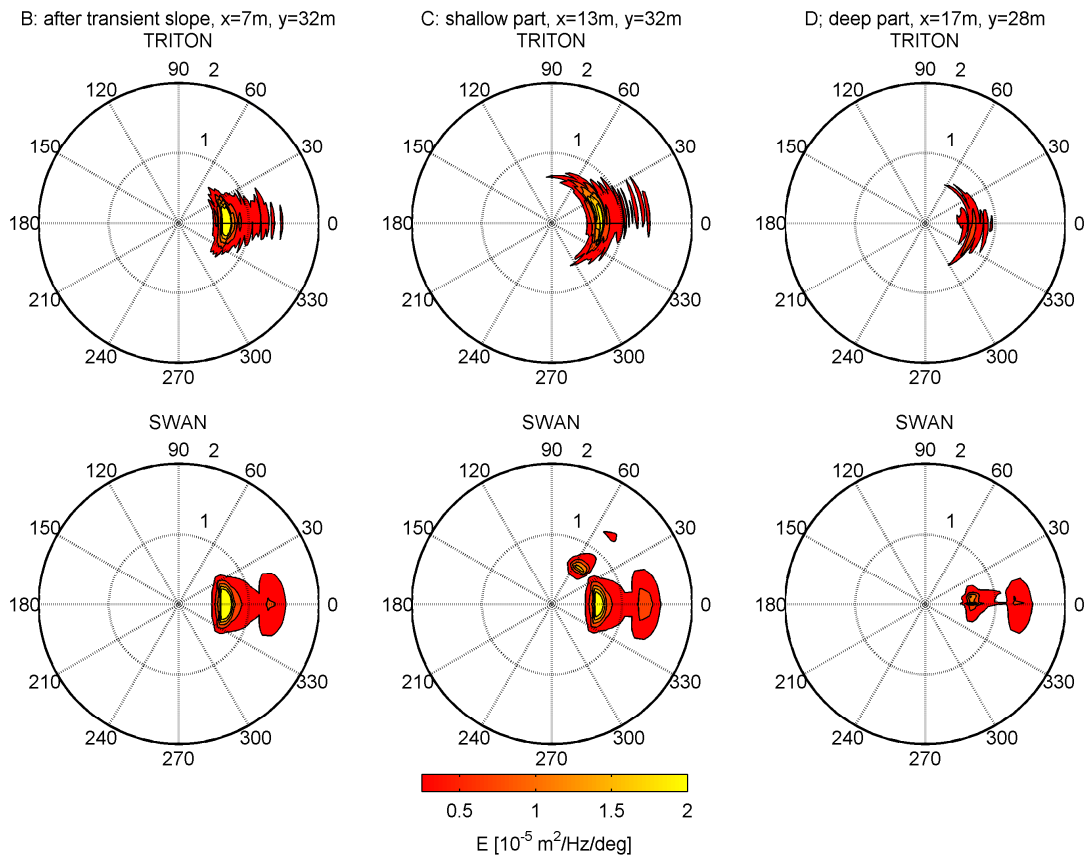


Figure 11: Variance density spectra for the simplified channel case ($H_{m0} = 0.082\text{m}$, $T_p = 1.45\text{s}$, dir. spr. = 20°), computed by TRITON (left column) and SWAN (right column) at the three locations in Figure 10.

The SWAN spectra show an additional peak at the primary frequency of 0.66 Hz at the directions of 40 – 50 degrees at location C. This is probably caused by the anti-focal point where the channel slope connects to the closed side wall (near $x = 6$ m, $y = 26$ m). TRITON also shows a broadening of the spectrum at the peak frequency, that may be caused by this anti-focal point as well. Nonetheless, the TRITON spectra are broader at this frequency and have less energy at the second harmonic. As already mentioned, both aspects are the result of the difference in nonlinear interactions, 1D super-

harmonic self-interactions in SWAN versus 2D sub- and super-harmonic interactions in TRITON. Additionally, the 2D spectra computed by TRITON are directionally broader in the deep region at location D. Thus, differences appear not only in the shallow region, but also in the deep region. This indicates that the nonlinear mechanism in TRITON not only influences the spectral shape in the shallow region, but also affects the transfer of energy across the channel slope into the deeper part thanks to the better representation of the spectrum in the shallow region.

Overall we can conclude that penetration of wave energy is reduced due to refraction at the flat-channel interface. The 2D super and sub-harmonic interactions in TRITON are spreading the energy over a range of frequencies and directions. As a consequence the wave attack angle at the flat-channel interface changes and part of the wave energy is no longer refractively trapped. On the other hand, SWAN's 1D nonlinear self-interaction triad formulation (LTA) overpredicts the energy transfer to the second harmonic in the shallow part, but is not able to transfer energy to other directions. Due to the lack of directional broadening SWAN underpredicts the amount of wave energy penetration into the channel, compared to TRITON.

5. CONCLUSIONS AND RECOMMENDATIONS

In storm hindcasts SWAN proved to underestimate the penetration of North Sea swell waves into the tidal basin of the Wadden Sea and Eastern Scheldt, which are complex areas with tidal flats and channels. It is well known that refraction is a dominant mechanism in swell wave propagation over complex areas with channels. Based on laboratory measurements and successive numerical computations with SWAN and the Boussinesq-type wave model TRITON the hypothesis was raised that 2D nonlinear interactions are an important mechanism that changes the energy density spectrum in such a way that additional wave energy is transmitted into and across channels.

From the results with the monochromatic and bi-chromatic waves we conclude that TRITON qualitatively reproduces the results of the parabolic model of Toledo (2013) for the single frequency, upslope case considered and that the conceptual idea of nonlinear interactions raised by Toledo (2013) has been confirmed: 2D sub- and super-harmonic nonlinear interactions broaden the variance density spectrum not only in frequency space but also in directional space, both in up-slope and down-slope situations.

SWAN's 1D nonlinear self-interaction triad formulation (LTA) does not include a mechanism to redistribute the energy over a wider range of directions. The absence of this directional broadening mechanism leads to an underestimation of the wave propagation across the channel. Whereas waves are hampered to enter the channel because of refraction, the nonlinear broadening mechanism may generate wave components under attack angles that are not refracted from the channel. The omission in SWAN is clearly relevant for harbor (entrances) and is most likely relevant for the swell penetration into the Wadden Sea towards the main land.

Obviously, SWAN's underestimation depends on the geometry of the channels, the wave directions, the spectral shape and the water depth. Additional investigations are still required in order to quantify and generalize the effect of nonlinear interactions on this transmission of energy. TRITON cannot replace SWAN in the wave prediction in large areas as the Wadden Sea. Essential wave physics, such as wind input, is lacking in a phase-resolving model as TRITON, and the computational cost for such large domain is too expensive. Therefore it is recommended to develop an alternative for the presently implemented 1D three-wave interaction formulation in SWAN.

ACKNOWLEDGMENTS

The research presented here is part of the WTI 2017 project ("Research and development of safety assessment tools of Dutch flood defences"), commissioned by the department WVW of Rijkswaterstaat in the Netherlands.

REFERENCES

- Booij, N., R.C. Ris and L.H. Holthuijsen. 1999. A third generation wave model for coastal regions: 1. Model description and validation. *J. Geophys. Res.*, 104 (C4), 7649-7666.
- Borsboom, M.J.A., N. Doorn, J. Groeneweg and M.R.A. van Gent. 2000. A Boussinesq-type model that conserves both mass and momentum. *Proceeding of 27th International Conference on Coastal Engineering*, ASCE, 148-161.

- Eslami S. A., A. van Dongeren, P. Wellens. 2012. Studying the effect of linear refraction on low-frequency wave propagation (physical and numerical study), *Proceedings of 33rd International Conference on Coastal Engineering*, ASCE.
- Groeneweg, J., M. van Gent, J. van Nieuwkoop and Y. Toledo. 2014. Wave propagation into coastal systems with complex bathymetries. Submitted for publication.
- Eldeberky, Y. (1996), Nonlinear transformations of wave spectra in the nearshore zone, Ph.D thesis, 203 pp., Delft Univ. of Technol., Delft, Netherlands.
- Herbers, T. H. C., S. Elgar, and R. T. Guza. 1995. Generation and propagation of infragravity waves, *J. Geophys. Res.*, 100 (C12), 24863–24872, doi:10.1029/95JC02680.
- Toledo, Y. 2013. The oblique parabolic equation model for linear and nonlinear wave shoaling. *J. Fluid Mech.*, 715, 103-133.
- Van der Westhuysen, A.J., A.R. van Dongeren, J. Groeneweg, G.Ph. van Vledder, H. Peters, C. Gautier, and J.C.C. van Nieuwkoop. 2012. Improvements in spectral wave modeling in tidal inlet seas. *J. Geophys. Res.*, 117, doi:10.1029/2011JC007837.
- Zijlema, M., G.Ph. van Vledder and L.H. Holthuijsen. 2012. Bottom friction and wind drag for wave models. *Coastal Engineering*, 59, doi:10.1016/j.coastaleng.2012.03.002.